Design and Comparison of Dual-Purpose Stator Windings for Active Chatter Suppression in Milling Spindles

Dennis Guhl, Robin Liebfried, and Wilfried Hofmann

Technische Universität Dresden, Chair of Electrical Machines and Drives, Dresden, Germany
dennis.guhl@tu-dresden.de,

Abstract

The effect of chatter is one of the main obstacles to increasing metal removal rates in modern high-speed cutting (HSC). Active damping approaches using electromagnetic actuators have gained popularity in recent years but none of them found significant industrial usage. One of the major drawbacks of the existing solutions is the missing geometrical and electrical integration which inevitably leads to a lengthening of the milling spindle inherently with lower rigidity values or a loss of power. In this paper, we aim for an approach without additional actuators. By using the concept of a bearingless motor to apply the damping forces onto the rotor, we achieve a fully geometrical and electrical integrated design. In addition, the implementation of a so-called dual-purpose or combined winding allows us to freely shift the total spindle power between torque and force generation which can lead to better-dimensioned spindle motors. The main premise is to keep high industrial proximity so that no geometrical changes are to be made to the motor, but the force generation is achieved solely by rewinding the stator. The chatter damping function shall always just be an extension of the drive function so that the new machine is never worse than the original one. After a pre-study, the two most promising dual-purpose windings—dual-purpose no-voltage and multiphase—are compared against the conventional separated windings design. The main evaluation criteria are a torque characteristic equivalent to the original motor and high radial forces with a low ripple for all rotor positions. The simulations are carried out as 2D finite element simulations at an uncontrolled machine. Many references between the separated and dual-purpose winding designs can be drawn. A multiphase approach with twelve phases in total works best with minimal changes to the original winding, an identical torque, and excellent force characteristics and leads to the commission of a prototype.

Frequently used variables

F_r	radial force	y_c	coil span
$\hat{i}_k$	amplitude of current system $\boldsymbol{i}_k$	z_s	number of turns per slot
k	phase-shift parameter	α	mech. angle along the motor circumference
m	number of phases		
N	number of slots	Θ_k	MMF caused by $\boldsymbol{i}_k$
n_i	winding distribution of phase i	ν	harmonic order of the winding distribution
$\hat{n}_\nu$	ν-th order Fourier coefficient of the winding distribution	$\varphi_{\mathrm{i}k}$	phase-angle of current system $\boldsymbol{i}_k$
p, p_s	pole pairs in the torque, suspension winding	$\varphi_{\mathrm{n}\nu}$	phase-angle of the ν-th order winding distribution harmonic
q	number of slots per phase	φ_r	mech. rotor revolution angle
t	time	ω	electrical angular frequency

1 Introduction

In today's high-speed milling, process instabilities are one of the main causes of productivity limitations [1]. In processes with high metal removal rates, chatter effects form the basis of these instabilities. Self-excited vibrations, called chatter, deteriorate the surface quality of the workpiece and lead to a reduction of the machine tool's life, especially the cutting tool [1]. Chatter vibrations belong to the self-excited vibrations. As with forced oscillations, an external energy source is necessary, but the process itself determines the rate of energy supply. The oscillation frequency follows from the dynamic properties of the process itself and cannot simply be influenced by the exciting force as in the case of forced oscillations.

The primary reason for chatter is the regenerative effect, which results from an interaction between the tooth engagement frequency and the vibration frequency of the cutting tool itself [2]. The chip thickness varies at each tooth engagement, depending on the current cutting tool position and on its position one revolution (single edge tools) or one engagement (multi-edge tools) before. The varying chip thickness, assuming a constant chip width, is accompanied by a varying thrust, which leads to vibrations of the machine tools and results in a closed-loop effect. At too high feed rates and/or cutting depths the process becomes unstable. Chatter marks are visible on the workpiece's surface like shown in Fig. 1. In most applications such a surface cannot be used and needs reworking.

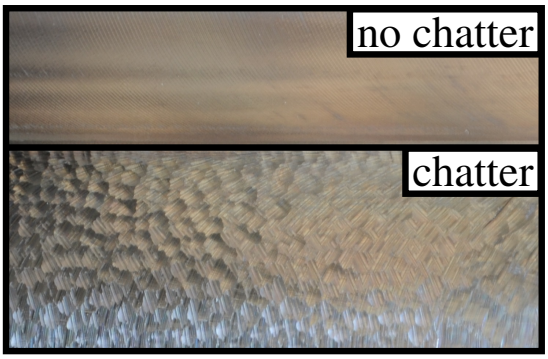

Figure 1: Chatter marks

Since the causes of chatter were discovered in the late 1950s, numerous methods have been investigated to suppress chatter. One of them are active damping techniques. These techniques are characterized by the measurement of one or more quantities characterizing the chatter vibration, the subsequent signal processing, the generation of control signals, and the actual force effect of the actuator on the process in a closed-loop control scheme. One can distinguish between series or parallel applications, depending on whether or not the actuator is subject to cutting forces [1]. There exist plenty solution approaches regarding an active structural chatter suppression [3]–[5], active tools (mostly focused on boring bars [6]) or workpiece holders [7].

This research focuses on actively damped spindle systems. Even in this subfield, two main groups of solutions can be distinguished. While some focus on the usage of active magnetic bearings [8], [9], others attempt to apply forces on the spindle axis at numerous different positions by other means. In many of the latter approaches piezoelectric actuators are used, for example, to apply forces directly on conventional contact bearings [10] or to manipulate the bearing's position [11].

In recent years electromagnetic actuators attracted attention. Abele et al. used an actuator next to the front bearing close to the milling tool [12]. Klaffert positioned the actuator in between the front bearing and the motor [13], while Bickel went for a split motor design [14]. Especially about the positioning of the actuator, far-reaching investigations were carried out. Positions between both mechanical bearings turned out to work best. But still, the volume of the additional actuator inevitably lengthens the milling spindle and therefore reduces the rigidity values. Alternatively, a corresponding reduction in the motor volume leads to a power and torque loss.

For this reason, Königsberg et al. developed a motor integrated actuator design [15]. Two main challenges need to be faced. Firstly, the integration leads to two harmonic spectrums—one for the motor,

one for the actuator stator winding—which need to be decoupled. Secondly, you need to model the achievable damping force as a function of the rotor position. Regardless of the significantly increased motor power with the same volume of the spindle, a force acting over the entire active length of the motor, and a reduced manufacturing effort compared to the other solutions presented above, this design still has one serious disadvantage: It is not possible to freely shift the motor and damping power back and forth. In a first publication 40 % of the total available copper cross-sectional area is used for the damping winding, 60 % for the motor winding [15] while in the latest publication (December 2020) the research group postulates a 25/75 ratio [16]. This approach reduces the torque also in operating points where no damping is required and more torque might be desirable.

The ability to freely shift the total available electric power between torque and damping force generation depending on the need at the specific operating point would be a clear advantage. Additionally, current spindle motors normally feature a double-layer design. This allows short-pitching of the coils to reduce harmonics and therefore the torque ripple. The proposed integrated actuator design just allows a single-layer motor winding with no possibility of short-pitching.

To achieve this goal, we take a different approach. The concept of a bearingless motor—here used for damping, not for suspension—can combine the advantages like force application over the entire active length of the motor and easy manufacturing of a fully integrated actuator as in [15] with the advantage of a free power shift. The idea to use bearingless motors for vibration suppression was already proposed in 2008 by Chiba et al. [17], but this method does not seem to have been applied in connection with industrial milling spindles yet. Especially, the free power shift represents a clear advantage over all other methods mentioned above.

Structure Section 2 presents the investigation setup including the evaluation criteria, the investigated winding designs, and details about the original spindle motor. A pre-study in section 3 of two different separated winding designs forms the basis of the investigation of two different dual-purpose winding approaches in sections 4 and 5. The paper concludes with a final comparison and an outlook in section 6.

2 Investigation Setup

The main premise is to achieve high industrial proximity. Due to the conservative design approaches in mechanical engineering, no geometric changes are to be made to the motor. For easy replacement, the damping functionality is to be achieved exclusively by rewinding the stator. This goes hand in hand with many advantages. The manufacturing effort stays low and under consideration of a constant maximum current density in the stator winding, the electromagnetic design should not be a considerable challenge.

2.1 Evaluation Criteria

To follow the main premise of achieving high industrial proximity the torque curve in an exclusively motor operating mode should vary as little as possible from the original torque curve or at least should be equivalent in mean value and ripple. This implies that the new machine will never be worse than the original machine in no-damping operation. The ripple of the load torque due to the cutting edges is normally significantly higher than the machine's cogging torque.

The force's mean value resp. ripple shall be as high resp. low as possible at an operation point where the nominal current is divided equally between torque and force generation. A small force ripple ensures a uniform damping behavior over all rotor positions and simplifies a subsequent force control if it is not necessary to take a dependency of the rotor angle into account. The chosen operating point corresponds to a milling process of S275JR steel using a 16 mm four flute end mill with a feed per tooth and revolution of 0.1 mm, a radial depth of cut of 16 mm and an axial depth of cut of 5 mm [18]. The investigations are deliberately carried out on an uncontrolled machine, as it should already exhibit advantageous behavior by itself. Considerations regarding the control system will be the subject of later publications.

2.2 Investigated Winding Designs

To allow a free power shift between torque and damping force generation, winding concepts known as dual-purpose windings are necessary. These windings combine the conventional separated motor and damping windings into one. There exist several different design solutions such as [19]–[23]. Due to the premise of not changing the geometry of the original motor, but rather achieving the damping operation solely by rewinding the stator, some solutions were ruled out. Others were tested only in very distant operating areas and/or power ranges, so that we finally chose a "dual-purpose no-voltage" winding (section 4) and a multiphase one (section 5) as they seemed the most promising.

Additionally the conventional approach of a separated single-layer suspension winding with $p_s = p \pm 1$ is investigated as a reference and presented first. Many parallels can be drawn from it to the dual-purpose windings.

2.3 Motor

The investigated spindle motor is a highly utilised four-pole permanent magnet synchronous motor with surface magnets. The stator has a three phase double-layer 7/9 short pitch winding with four parallel branches per phase. Table 1 provides an overview of some of the motor specifications.

Table 1: Motor specifications

symbol	quantity	value
U_N	nominal voltage	308 V
I_N	nominal current	55 A
P_N	nominal power	25 kW
n_N	nominal speed	10 000 min^{-1}
n_max	maximum speed	20 000 min^{-1}
p	pole pairs	2

All simulations are carried out as 2D-FE simulations in ANSYS Maxwell. We consider saturation inside the electric steel M270-35A but neglect hysteresis and eddy current losses. We assume a linear magnet model with nominal remanence and coercivity values at 20 °C.

3 Separated Windings

The basic functional principle of the bearingless motor (here used for damping, not bearing) is based on the superposition of two magnetic fields with different pole pair numbers in the air gap of the motor, so that a defined torque and force are created via the Maxwell stress tensor. In bearingless PMSM (BLPMSM) the desired superposition for torque/force is between the rotor magnetic field and the respective stator one. Conventional bearingless motors contain two separate winding systems which pole pair numbers usually differ by one [24]

$$p_\mathrm{s} = p \pm 1. \tag{1}$$

The original motor has two pole pairs $p = 2$. So the pole pair of the suspension winding can be $p_\mathrm{s} = 1$ or $p_\mathrm{s} = 3$, respectively.

Fig. 2 shows the simulated torque and force characteristics over one full rotor revolution for $p_\mathrm{s} = 1$ and $p_\mathrm{s} = 3$. As mentioned above, the original nominal current is divided equally between the two windings so

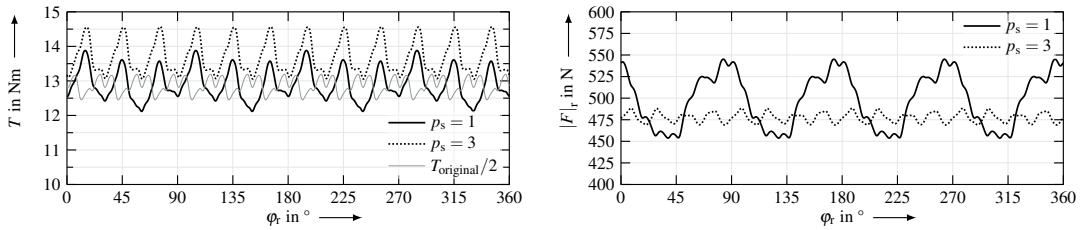

(a) (b)

Figure 2: Simulated (a) torque and (b) force characteristics of the conventional BLPMSM with separated windings

that the maximum current density remains the same. You can see that the torque's mean value has, as expected, nearly halved compared to the original motor, whereby the torque for $p_s = 1$ is lower due to saturation effects. The ripple increases significantly because of the missing short-pitching as the double layer winding turned into a single-layer one to create space for the force winding. The influences of the slot harmonics are visible in both torque and force. The mean value of the force magnitude is slightly higher for $p_s = 1$ (494 N) than for $p_s = 3$ (478 N), although the force ripple is disproportionately higher in the first case (18.5 % resp. 4 %). The reason for this is the high saturation of the original machine. Using a six-pole damping winding, the air gap fields of the PM and the damping winding are more evenly superposed than with a two-pole configuration, so that the electrical steel in the rotor and stator is less saturated. The dominant fourth-order force harmonic ($p_s = 1$) can therefore be traced back to the four-pole rotor magnetic field, whereas the dominant 16th-order harmonic ($p_s = 3$) is based on the superposition of the harmonics of the PM and damping winding fields. The significant beat in the torque characteristic for $p_s = 1$ can also be traced back to saturation effects.

Even though $p_s = 3$ seams more suited, both designs shown above shall be used as a reference for the approaches presented next. Since you need to decide on the winding distribution before manufacturing the motor, it does not suit the required free power shift, which is the major drawback of the separated windings design.

4 Dual-purpose no-voltage winding

Khoo proposed a bearingless motor design with a combined torque and suspension winding by the use of bridge connections in [25]. This design requires only one three-phase inverter for torque generation and one isolated H-bridge for each suspension phase. The bridge connections ensure that the suspension terminals do not see any back-EMF and corresponding inverters can be dimensioned substantially smaller or have increased control dynamics compared to other combined bearingless motor designs [22]. There is also the possibility to short-circuit the suspension terminal coils to get fully passive damping.

In [26] Chiba et. al. developed a bearingless motor design with a combined torque and suspension winding for vibration suppression. Due to the middle-point-current injection, there are only two three-phase inverters necessary, one for torque and one for suspension. This idea was refined by Oishi et. al. in [27] so that the suspension terminals experience no back-EMF. Hence, both winding designs, the one by Khoo and the one by Oishi et. al., have the same two main characteristics: a combined winding for torque and force generation as well as suspension terminal connections which see no back-EMF.

This led Severson et. al. [28] to introduce the term "dual-purpose no-voltage" (DPNV) windings which sums up these two main characteristics. Followed by results of the practical implementation of such a winding design in an ac homopolar motor in [29], Severson et. al. generalized the design theory for DPNV windings in [23] and proposed practical design guidelines.

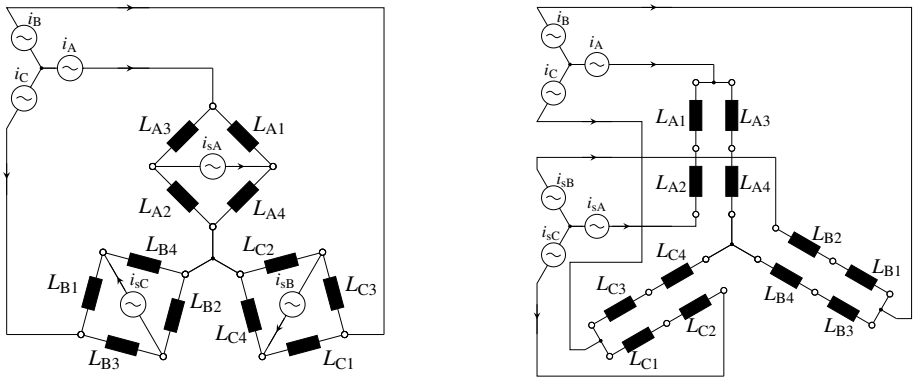

Figure 3: Bridge (a) and parallel (b) design of a DPNV winding (based on [23])

4.1 Design process

Both types of DPNV windings, the one with bridge connections [25] and the one with parallel connections [27] are depicted in Fig. 3. A comparison regarding the practical implementation of these two types is given in [29].

The parallel configuration was chosen as both three-phase inverters can be fed by isolated DC-buses. On the one hand, it counteracts any concerns regarding circulating currents, allows the conventional space vector modulation, and reduces the necessary amount of current sensors to four [29], on the other hand, it enhances the possibility to investigate the influence of the suspension inverter dynamics on the control scheme. All in all twelve switches and two isolated DC-buses are required, compared to 18 switches and four DC-buses in the bridge configuration which lead to lower hardware costs. Advantages of the bridge configuration regarding the fault redundancy were not considered in this evaluation as the motor to be manufactured will be a prototype.

The design process of a DPNV winding, starting from a conventional motor winding, is extensively covered in [23]. The following section only presents the main design steps for general understanding. For deeper insights into the design process, please refer to the denoted literature.

According to [23] there are restrictions to the relations between the number of stator slots N, the motor pole pair p and the suspension pole pair p_s. These restrictions lead to three conditions that must be fulfilled to make the conversion of a conventional winding into a DPNV winding possible.

The *first condition* checks for the symmetry of the torque winding. The number of phases m must be relatively prime to the pole pair of the torque winding as well as to the pole pair of the suspension winding:

$$p \perp m \quad \wedge \quad p_s \perp m. \tag{2}$$

The standard choice of $m = 3$ and the specification $p = 2$ allows only $p_s = 1$ for the suspension winding (see eqs. (1) and (2)).

The *second condition* ensures the fulfillment of the no-voltage requirement. For the given original stator winding with $N = 36$ slots the no-voltage requirement is already inherently fulfilled, so that we must only check for a sufficient amount of coils, which is obviously the case.

$$\frac{N}{4m} = 3 \in \mathbb{N}. \tag{3}$$

The *third condition* checks for a non-zero suspension winding factor. According to [23] the winding here represents a "type 1" winding and therefore one must check if the pole pair number of the motor winding is even

$$p = 2 \in \mathbb{N}_{\text{even}}. \tag{4}$$

When fulfilling all three conditions, what we do, it is possible to redesign the original motor winding into a DPNV one. The starting point is the star of slots of the motor winding, depicted in Fig. 4a. Therefrom, the connection star of slots is drawn as one-half of opposite voltage phasors have to be turned by 180° so that the winding becomes symmetrical and the distribution factor becomes non-zero (see Fig. 4b).

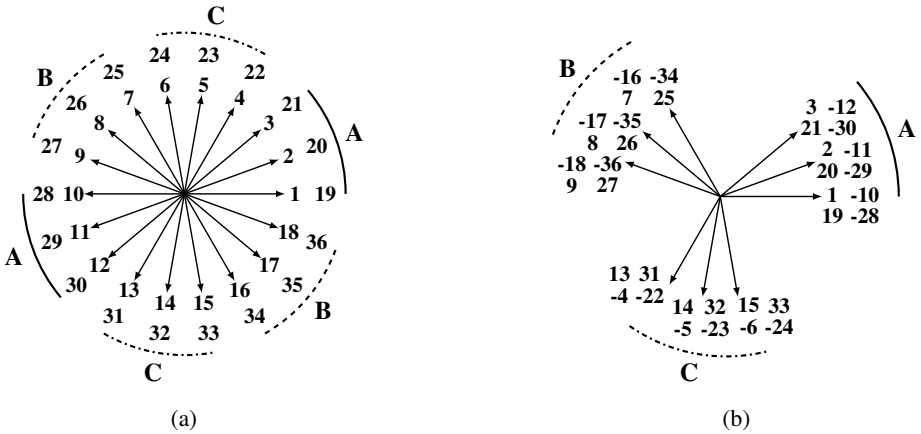

(a) (b)

Figure 4: Star of slots (a) and connection star of slots (b) of the torque winding

For self-compensation of the back-EMF at the suspension terminals ("no-voltage"), half of the coils need to be reversed. To determine the correct coils one redraws the connection star of slots for each phase at the suspension frequency (see Fig. 5). For a "type 1" winding any 180° band would work (grey semi-circle). But not all combinations result in a symmetrical connection star of slots of the suspension winding [23]. Using the star of slots in Fig. 6a one can project the position of the connection phasors. The resulting connection star is shown in Fig. 6b. Compared to the one of the motor winding in Fig. 4b phases B and C are interchanged, which has to be taken into account when specifying the suspension currents.

To finalize the design process the coils have to be assigned to the coil groups 1-4, see Fig. 3b. The corresponding slots of the lower layer can be obtained from the chosen coil span. The following two

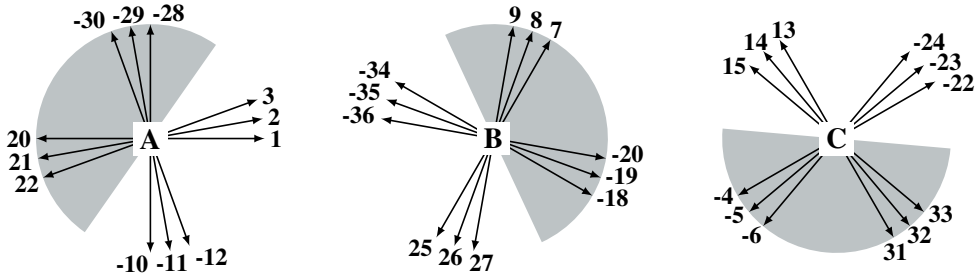

Figure 5: Connection stars of slots of the motor winding at suspension frequency (based on [23])

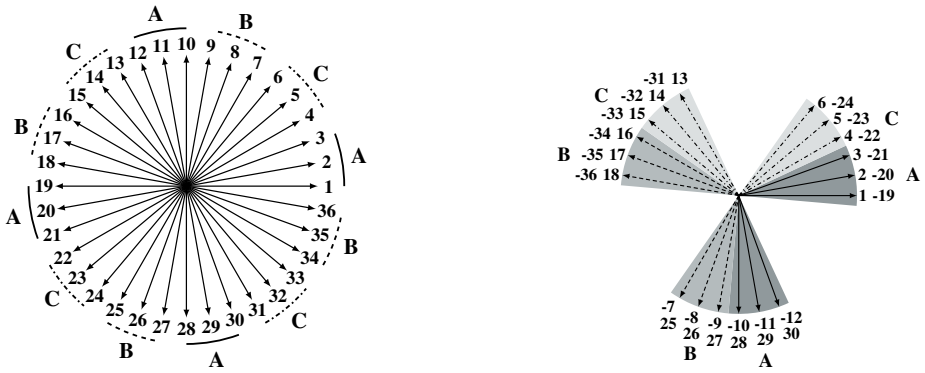

(a) (b)

Figure 6: Star of slots (a) and connection star of slots (b) of the suspension winding

paragraphs will compare a full pitch and a 7/9-short pitch configuration with each other as well as with the standard BLPMSM with $p_s = 1$ from section 3.

4.2 Simulation results

The simulated torque and force characteristics of the two DPNV designs over one full rotor revolution can be found in Fig. 7. The original nominal current is again divided equally between the torque and force generation (see section 3). One can see that the torque characteristics of the short pitch DPNV and the original motor are almost identical. This is expected as just the coil arrangement within a phase has changed but nothing else. The little deviations in uncontrolled operation result from the superposed suspension field. In an exclusive torque operation mode, the torque stays the same. The torque characteristic of the full pitch winding corresponds well to the one with separated windings (see Fig. 2). Due to the full pitch the torque mean value is higher compared to the short pitch design (13.5 Nm to 12.8 Nm) but also the ripple is significantly increased (12.4 % to 6.2 %). The characteristic beat is also clearly visible, although it is much less pronounced for the short pitched winding.

The force characteristics are very similar to the separated winding design with $p_s = 1$ as well, but the mean values have nearly halved for the full pitch winding (267 N) and have even more than halved for the short pitch one (217 N). The absolute force ripples stayed almost the same but the relative ones doubled due to the halved mean value (35.2 % resp. 45 %). An explanation therefore can be found in Fig. 8. As the suspension current distribution in the subfigure's upper parts shows, half of the suspension current is wasted in terms of MMF production to turn an original four-pole field into a two-pole field (see

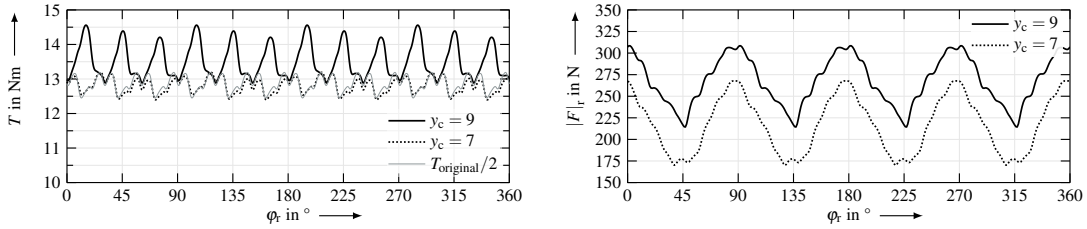

(a) (b)

Figure 7: Simulated force (a) and torque (b) characteristics of the full and short pitch DPNV bearingless motor over one rotor revolution

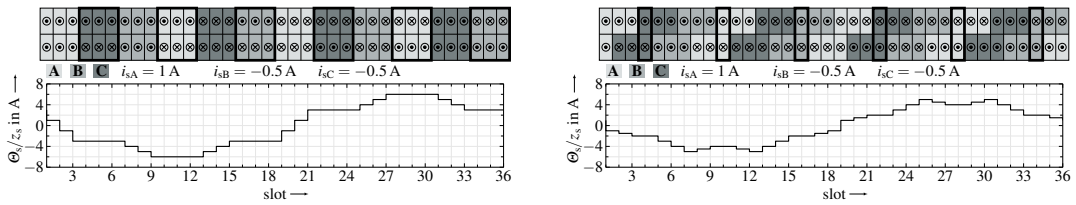

(a) $y_c = 9$ (b) $y_c = 7$

Figure 8: 1-dimensional suspension MMF of the full (a) and short pitch (b) DPNV bearingless motor

black rectangles). The suspension MMF characteristic looks even worse for the short pitch design and explains the lower mean value.

Investigations for different suspension current space vectors (rotated stepwise by 22.5°) in Fig. 9 show a similar behavior for all simulated space vector orientations. The black curves correspond to the ones in Fig. 7 and can be treated as a worst-case. Because of the low pole pair number of the suspension air gap field, the superposition with the PM field is more unevenly and results in higher force ripples (see section 3).

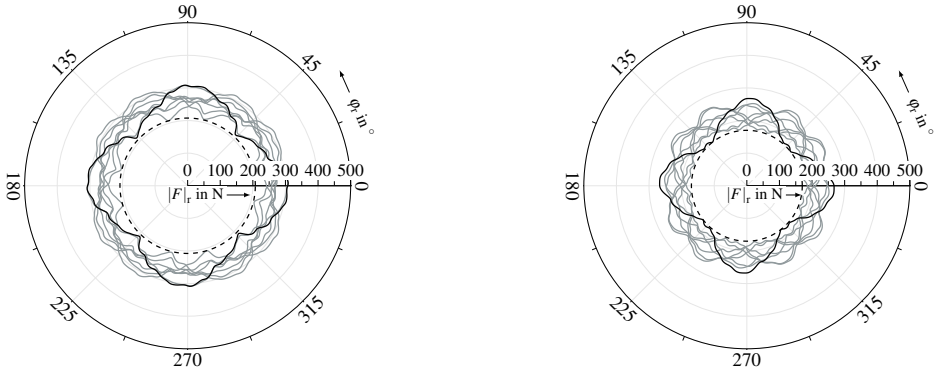

(a) $y_c = 9$ (b) $y_c = 7$

Figure 9: Simulated force and torque characteristics of the full (a) and short pitch (b) DPNV bearingless motor for different suspension current space vectors over one rotor revolution

All in all, the DPNV winding approach does not seem to suit the investigated highly utilized spindle motor if one is interested in high suspension/damping forces as half of the suspension current is just used to create a two-pole suspension field and is therefore wasted MMF wise. The suspension pole pair is fixed to $p_s = p - 1$, which leads to a worse behavior for high speeds in general [30]. This unsuitability may also count for HSC spindle motors in general as, due to the high rotational speeds, the most common numbers of pole pairs are $p = 2$ resp. $p = 3$.

5 Multiphase winding

Another realization of a dual-purpose winding is given by a research group around Kang. In various publications [22], [31], [32] they applied multiphase machine theory [33] to design a multiphase bearingless motor. The general idea is to superpose two different stator current systems and to specifically influence the fundamental and harmonic waves of the magnetic air gap field by carefully combining the

three central degrees of freedom of this winding design: number of phases, phase shift between the stator currents, and coil span. The winding distribution n_i can be expressed as a Fourier series

$$\begin{aligned} n_{\mathrm{A}}(\alpha) &= \sum_{\nu=1}^{\infty} \hat{n}_\nu \cos(\nu\alpha + \varphi_{\mathrm{n}\nu}) \\ n_{\mathrm{B}}(\alpha) &= \sum_{\nu=1}^{\infty} \hat{n}_\nu \cos\left(\nu\left(\alpha - \frac{2\pi}{m}\right) + \varphi_{\mathrm{n}\nu}\right) \\ &\vdots \\ n_{\mathrm{m}}(\alpha) &= \sum_{\nu=1}^{\infty} \hat{n}_\nu \cos\left(\nu\left(\alpha - (m-1)\frac{2\pi}{m}\right) + \varphi_{\mathrm{n}\nu}\right). \end{aligned} \tag{5}$$

One can see that the phase windings are distributed equally along the circumference whereas each phase itself is in general not symmetrical (see Fig. 10). Unlike conventional symmetrical three-phase stator windings, $\hat{n}_\nu$ exists for even harmonics as well (except full pitch multiphase windings). In this context, a full pitch means a coil span of half of the stator's circumference.

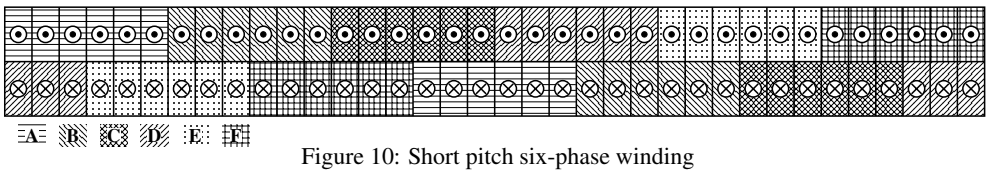

Figure 10: Short pitch six-phase winding

The phase currents are assumed to be totally sinusoidal

$$\boldsymbol{i}_k = \begin{bmatrix} i_{\mathrm{A}k} \\ i_{\mathrm{B}k} \\ \vdots \\ i_{mk} \end{bmatrix} = \hat{i}_k \begin{bmatrix} \cos(\omega t + \varphi_{\mathrm{i}k}) \\ \cos\left(\omega t + \varphi_{\mathrm{i}k} - k\frac{2\pi}{m}\right) \\ \vdots \\ \cos\left(\omega t + \varphi_{\mathrm{i}k} - (m-1)\,k\frac{2\pi}{m}\right) \end{bmatrix} \tag{6}$$

where k determines the current's phase shift. The resulting MMF $\boldsymbol{\Theta}_k$ for $\boldsymbol{i}_k$ is:

$$\boldsymbol{\Theta}_k(\alpha,t) = \sum_{\xi=1}^{m} \left[\underbrace{\hat{i}_k \cos\left(\omega t + \varphi_{\mathrm{i}k} - (\xi-1)\,k\frac{2\pi}{m}\right)}_{\text{current}} \cdot \sum_{\nu=1}^{\infty} \underbrace{\hat{n}_\nu \cos\left(\nu\left(\alpha - (\xi-1)\frac{2\pi}{m}\right) + \varphi_{\mathrm{n}\nu}\right)}_{\text{winding}} \right]. \tag{7}$$

Applying $\cos(x)\cdot\cos(y) = \frac{1}{2}(\cos(x-y)+\cos(x+y))$ one can describe the ν-th MMF harmonic caused by $\boldsymbol{i}_k$ as

$$\boldsymbol{\Theta}_{k\nu} = \begin{cases} \frac{\hat{i}_k \hat{n}_\nu}{2} \cos(\omega t + \varphi_{\mathrm{i}k} + \nu\alpha + \varphi_{\mathrm{n}\nu}) & \text{for } k+\nu = l\cdot m \\ 0 & \text{for } k \pm \nu \neq l\cdot m \\ \frac{\hat{i}_k \hat{n}_\nu}{2} \cos(\omega t + \varphi_{\mathrm{i}k} - \nu\alpha + \varphi_{\mathrm{n}\nu}) & \text{for } k-\nu = l\cdot m \end{cases} \tag{8}$$

with $l \in \mathbb{Z}$ [22]. It is now possible to evaluate (8) for various combinations of number of phases and phase shifts.

As the number of slots per phase q shall be an integer, the number of phases is restricted to $m = 6,9,12,18$. Fig. 11a shows the evaluation of (8) for a six-phase motor. Each stator current system evokes forward and backward rotating or pulsating harmonics. We will focus on the upper $(m/2-1)$-rows as the bottom half is mirrored with reversed rotating directions. If m is even, the $m/2$-th and m-th row (phase shifts of π resp. 2π) just cause pulsating field waves which are useless for force and torque generation. The bottom row displays the harmonics of the magnetic field caused by the permanent magnets. Torque is generated by the interaction of a harmonic of the PM-field and a harmonic of the same order caused by the stator currents. Only the fundamental waves ($\nu = p = 2$) cause a useful torque. All interactions by higher harmonics result in alternating torque just producing torque ripple. So the intention is to minimize these interactions by diminishing the respective harmonic components n_ν of the stator MMF. The same applies to the generation of force. Every $(p(2l+1)\pm 1)$-th ($l \in \mathbb{N}$) rotating current harmonic interacts with the PM-harmonics ($p(2l+1)$, $l \in \mathbb{N}$) generating force effects whereas only the fundamental harmonics contribute a useful force component and the higher ones just enhance the force ripple. Special attention must be paid to the force-generating interactions between the harmonics of different stator current systems (e.g. $\boldsymbol{i}_{k=1}$ and $\boldsymbol{i}_{k=2}$, see black rectangles in Fig. 11a). Generally speaking, an increase of the number of phases leads to a more equalized harmonic spectrum.

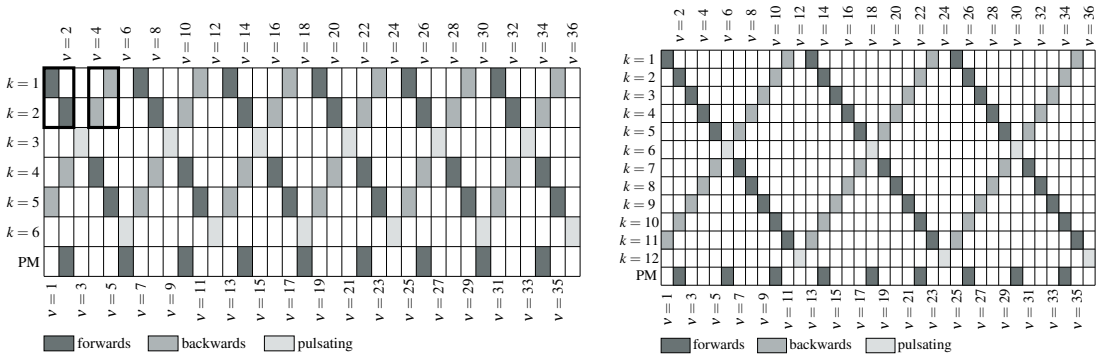

(a) $m = 6$ (b) $m = 12$

Figure 11: Evaluation of the MMF harmonics of a six (a) and twelve (b) phase motor (based on [22])

An analytical expression for the harmonic components of the stator MMF is therefore needed. We will assume just a radial MMF (1D-representation) caused by windings concentrated in the middle of each slot. A more detailed description as e.g. the 2-D approach in [34] is not necessary as the basic relationships already become clear in a 1D representation and are sufficient for the choice of the number of phases and the coil span.

We can decompose the winding distribution into two sums of step functions:

$$\begin{aligned} n_{\mathrm{A}}(\alpha) &= n_{\mathrm{up\,A}}(\alpha) + n_{\mathrm{dw\,A}}(\alpha) \\ &= z_{\mathrm{s}} \sum_{l=1}^{q} \mathbb{1}\left(\alpha - (l-1)\frac{2\pi}{N}\right) - z_{\mathrm{s}} \sum_{l=1}^{q} \mathbb{1}\left(\alpha - ((l-1)+y_{\mathrm{c}})\frac{2\pi}{N}\right). \end{aligned} \tag{9}$$

Combined with the Fourier expansion of the shifted step function

$$\mathbb{1}(\alpha-\varphi) = 1 - \frac{\varphi}{2\pi} + \frac{1}{\pi}\sum_{\nu=1}^{\infty}\left[-\frac{\sin(\nu\varphi)}{\nu\pi}\cos(\nu\alpha) + \frac{\cos(\nu\varphi-1)}{\nu\pi}\sin(\nu\alpha)\right] \tag{10}$$

and the superposition of harmonic oscillations with same frequency, this leads to the Fourier coefficients in (5).

5.1 Design process

Since there are four different numbers of phases possible, a preselection had to be made. The bearingless operation relies on the superposition of two different current systems. From Fig. 11 one can see that $\boldsymbol{i}_{k=2}$ is necessary for torque generation and $\boldsymbol{i}_{k=2}$ or $\boldsymbol{i}_{k=3}$ — equivalent to $p_\mathrm{s} = 1$ resp. $p_\mathrm{s} = 3$ — for force generation (for $m = 6$ only $\boldsymbol{i}_1$). This superposition results in unsymmetrical phase currents so that an H-bridge is needed for each phase. A choice of $m = 18$ would therefore result in a disproportionately high need of switches. Initial studies showed an unfavourable force and torque characteristic for $m = 9$ due to an undesirable interaction between the magnetic fields' second harmonic, so that the design process focus on $m = 6$ and $m = 12$.

Fig. 12 shows the scaled Fourier coefficients of the winding distribution for six and twelve phases from eqs. (9) and (10). The vertical dashed lines indicate the chosen coil spans for $p_\mathrm{s} = 1$ (black) and for $p_\mathrm{s} = 3$ (grey), respectively. These choices represent a good compromise between a sufficiently high generation of torque and force (see fundamental harmonics) and also a minimization of the critical higher-order coefficients. For example for $m = 6$ the 5,7,11,13,...-th order harmonics of $\boldsymbol{i}_1$ will interact with the PM harmonics and cause undesired force ripples. The same counts for the 4,8,10,14,...-th orders harmonics of $\boldsymbol{i}_2$ in interaction with the harmonic spectrum of $\boldsymbol{i}_1$. Since lower harmonics tend to have a greater influence we focus for this example on $\nu = 1,2,4,5$. The product of $\hat{n}_1$ and $\hat{n}_2$ shall be as large as possible whereas $\hat{n}_4$ and $\hat{n}_5$ shall be as small as possible at the same time. For a coil span of nine $\hat{n}_4$ becomes zero and $\hat{n}_5$ rather small and $\hat{n}_2$ maximal, but this choice leads to a considerable loss of force generation as $\hat{n}_1$ is far from optimal. A coil span of eleven, on the other hand, provides a significant increase of $\hat{n}_1$, just a small decrease of $\hat{n}_2$ and $\hat{n}_4$ as well as $\hat{n}_5$ stays reasonably low.

Fig. 12b indicates a much higher force generation by $\boldsymbol{i}_1$ than by $\boldsymbol{i}_3$ but this only counts for a linear machine. The spindle motor is highly utilized and therefore even under normal operation considerably saturated, so that the resulting force is approximately equal. The chosen coil span for $m = 12$, $p_\mathrm{s} = 3$ corresponds exactly to the original winding.

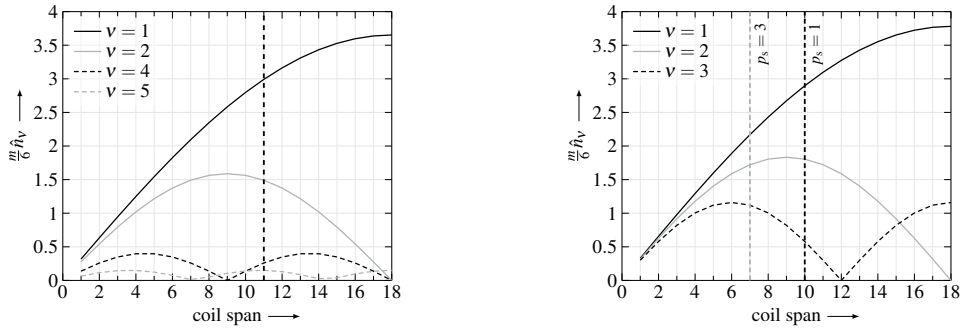

(a) $m = 6$ (b) $m = 12$

Figure 12: Scaled Fourier coefficients for six (a) and twelve (b) phase windings

5.2 Simulation results

We carried out the same simulations for the multiphase bearingless motors as we did in section 4.2. The torque and force characteristics are shown in Fig. 13. The former have a very even course, whereby the torque for $m = 6$ still shows some noticeable influences of a fourth order harmonic and the distinctive beat (see section 3). Its mean value (10.7 Nm) is, as indicated by Fig. 12, lower than the one for $m = 12$ (12.9 Nm). For the torque ripple it is, due to the influence of the fourth order harmonic and the lower

mean value, just the other way round (7.6 % resp. 5.4 %). As the twelve-phase winding corresponds to the original one, the torque characteristics are nearly identical. The small deviations in uncontrolled operation are caused by the superposed suspension field. In an exclusively torque operating mode the torque will be the same.

The force characteristics show a very familiar behavior to the separated winding designs. Using a six-phase motor the force has a very dominant fourth order harmonic and a very large ripple of 25.1 %. Its mean value of 412.6 N is, compared to section 3, even a bit lower than the one of 430.8 N of the twelve-phase motor which has a ripple of just 2.8 %.The results for $m = 12$ with $p_s = 1$ are not shown here as they just represent a undesirable combination of the torque characteristic of the twelve-phase motor with $p_s = 3$ and the force characteristic of the six-phase motor.

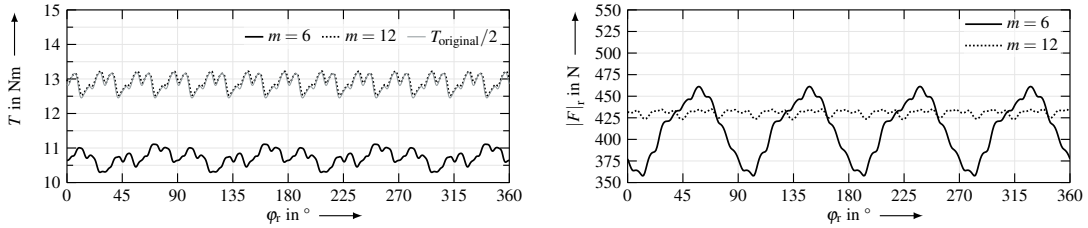

(a) (b)

Figure 13: Simulated force (a) and torque (b) characteristics of the six- and twelve-phase bearingless motor over one rotor revolution

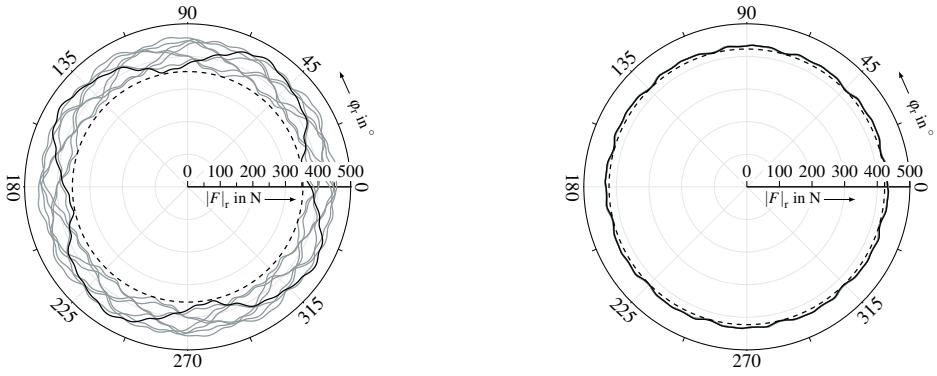

(a) $m = 6$ (b) $m = 12$

Figure 14: Simulated force and torque characteristics of the six (a) and twelve (b) phase bearingless motor for different suspension current space vectors over one rotor revolution

Fig. 14 confirms the excellent force characteristic of the twelve-phase motor. The same simulations as in Fig. 9 were carried out for the multiphase motors. The deviations in force magnitude for different suspension current space vectors are so small that they are barely depictable in this figure. The six-phase motor in Fig. 14a shows a similar behavior as the DPNV designs in Fig. 9 as all of them correspond to $p_s = 1$.

6 Conclusion

DPNV windings present in general a valid approach to turn standard motors into bearingless ones with low demand for power electronics, but they prove to be unsuitable for the spindle motor investigated here and HSC spindle motors with pole pairs of $p = 2$ and $p = 3$ in general.

The multiphase approach leads to significantly better results at the cost of high demand for power electronics. A twelve-phase motor with $p_s = 3$ worked best. The stator winding is equivalent to the original one just with the difference that the once parallelized coil groups in each phase are now supplied each by an own H-bridge. Therefore, in normal operation mode, the torque characteristic is identical to the original motor. The investigations above also show an excellent force characteristic even at an uncontrolled state.

Generally speaking, a two-pole suspension field ($p_s = p - 1$) leads to worse torque and force characteristics than a six-pole one ($p_s = p + 1$) due to the interactions of the specific harmonic spectrums and therefore a more evenly superposition of the suspension and the rotor field. This goes hand in hand with the results from [30], [35] and even ensures lower rotor eddy-current losses which were not addressed in this paper.

Based on these findings, a twelve-phase prototype was commissioned. The practical investigation and control scheme of this bearingless spindle motor is the subject of further publications.

Acknowledgments The authors would like to thank the "Sächsische Aufbaubank" (SAB) and the European Union (EU) for funding this research under the European Regional Development Fund (ERDF) with SAB application no. 100348076.

References

[1] J. Munoa, X. Beudaert, Z. Dombovari, *et al.*, "Chatter suppression techniques in metal cutting," *CIRP Annals*, vol. 65, no. 2, pp. 785–808, 2016.

[2] S. A. Tobias and W. Fishwick, "Theory of regenerative machine tool chatter," *The Engineer*, vol. 205, no. 7, pp. 199–203, 1958.

[3] A. Cowley and A. Boyle, "Active dampers for machine tools," *CIRP Annals*, vol. 18, no. 2, pp. 213–222, 1970.

[4] J. Munoa, X. Beudaert, K. Erkorkmaz, *et al.*, "Active suppression of structural chatter vibrations using machine drives and accelerometers," *CIRP Annals*, vol. 64, no. 1, pp. 385–388, 2015.

[5] E. Abele, M. Roth, C. Ehmann, *et al.*, "Aktiver Strukturdämpfer. Dimensionierung, Konstruktion und Verifikation an einem Bearbeitungszentrum," German, *wt Werkstatttechnik online*, vol. 100, pp. 105–111, 2010.

[6] H. Tanaka, F. Obata, T. Matsubara, *et al.*, "Active chatter suppression of slender boring bar using piezoelectric actuators," *JSME International Journal. Ser. C, Dynamics, control, robotics, design and manufacturing*, vol. 37, no. 3, pp. 601–606, 1994.

[7] C. Brecher, D. Manoharan, U. Ladra, *et al.*, "Chatter suppression with an active workpiece holder," *Production Engineering*, vol. 4, no. 2-3, pp. 239–245, 2010.

[8] C. R. Knospe, "Active magnetic bearings for machining applications," *Control Engineering Practice*, vol. 15, no. 3, pp. 307–313, 2007.

[9] J.-H. Kyung and C.-W. Lee, "Controller design for a magnetically suspended milling spindle based on chatter stability analysis," *JSME International Journal. Ser. C, Mechanical systems, machine elements and manufacturing*, vol. 46, no. 2, pp. 416–422, 2003.

[10] M. Ries and S. Pankoke, "Increasing the stability of the milling process by an active milling spindle," in *Proceedings of the 1st international conference on process machine interactions*, 2008, pp. 95–102.

[11] P. Albertelli, S. Elmas, M. R. Jackson, *et al.*, "Active spindle system for a rotary planing machine," *The International Journal of Advanced Manufacturing Technology*, vol. 63, no. 9-12, pp. 1021–1034, 2012.

[12] E. Abele, R. Nordmann, C. Ehmann, *et al.*, "Aktive Motorspindel stabilisiert den Prozess," German, *Werkstatt und Betrieb*, vol. 138, no. 11, pp. 22–27, 2005.

[13] T. Klaffert, *Selbstoptimierende HSC-Motorspindel*, German. Verlag Wissenschaftliche Scripten, 2006.

[14] W. Bickel, *Frässpindel mit motorintegrierter aktiver Dämpfung*, German. PZH Verlag, 2015.

[15] J. Königsberg, J. Reiners, B. Ponick, *et al.*, "Highly dynamic spindle integrated magnet actuators for chatter reduction," *International Journal of Automation Technology*, vol. 12, no. 5, pp. 669–677, 2018.

[16] B. Denkena, B. Bergmann, and F. Böhse, "Mechatronic damping systems as enablers for autonomous machine tools," *Proceedings of the Machining Innovations Conference (MIC) 2020*, pp. 166–173, 2020.

[17] A. Chiba, T. Fukao, and M. A. Rahman, "Vibration suppression of a flexible shaft with a simplified bearingless induction motor drive," *IEEE Transactions on Industry Applications*, vol. 44, no. 3, pp. 745–752, 2008.

[18] O. Kienzle, "Die Bestimmung von Kräften und Leistungen an spanenden Werkzeugen und Werkzeugmaschinen," German, *VDI-Zeitschrift*, vol. 94, no. 11–12, pp. 299–305, 1952.

[19] D. Dietz, G. Messager, and A. Binder, "1 kW/60,000 min^{-1} bearingless pm motor with combined winding for torque and rotor suspension," *IET Electric Power Applications*, vol. 12, no. 8, pp. 1090–1097, 2018.

[20] S. Kobayashi, M. Ooshima, and M. N. Uddin, "A radial position control method of bearingless motor based on d-q-axis current control," *IEEE Transactions on Industry Applications*, vol. 49, no. 4, pp. 1827–1835, 2013.

[21] W. Gruber, W. Amrhein, and M. Haslmayr, "Bearingless segment motor with five stator elements—design and optimization," *IEEE Transactions on Industry Applications*, vol. 45, no. 4, pp. 1301–1308, 2009.

[22] M. Kang, J. Huang, J.-q. Yang, *et al.*, "Analysis and experiment of a 6-phase bearingless induction motor," in *2008 International Conference on Electrical Machines and Systems (ICEMS)*, IEEE, 2008, pp. 990–994.

[23] E. L. Severson, R. Nilssen, T. Undeland, *et al.*, "Design of dual purpose no-voltage combined windings for bearingless motors," *IEEE Transactions on Industry Applications*, vol. 53, no. 5, pp. 4368–4379, 2017.

[24] A. Chiba, T. Fukao, O. Ichikawa, *et al.*, *Magnetic Bearings and Bearingless Drives*. Elsevier, 2005.

[25] W. K. S. Khoo, "Bridge configured winding for polyphase self-bearing machines," *IEEE Transactions on Magnetics*, vol. 41, no. 4, pp. 1289–1295, 2005.

[26] A. Chiba, K. Sotome, Y. Iiyama, *et al.*, "A novel middle-point-current-injection-type bearingless pm synchronous motor for vibration suppression," *IEEE Transactions on Industry Applications*, vol. 47, no. 4, pp. 1700–1706, 2011.

[27] R. Oishi, S. Horima, H. Sugimoto, *et al.*, "A novel parallel motor winding structure for bearingless motors," *IEEE Transactions on Magnetics*, vol. 49, no. 5, pp. 2287–2290, 2013.

[28] E. L. Severson, R. Nilssen, T. Undeland, *et al.*, "Dual-purpose no-voltage winding design for the bearingless ac homopolar and consequent pole motors," *IEEE Transactions on Industry Applications*, vol. 51, no. 4, pp. 2884–2895, 2015.

[29] E. L. Severson, S. Gandikota, and N. Mohan, "Practical implementation of dual-purpose no-voltage drives for bearingless motors," *IEEE Transactions on Industry Applications*, vol. 52, no. 2, pp. 1509–1518, 2016.

[30] T. Schneider, J. Petersen, and A. Binder, "Influence of pole pair combinations on high-speed bearingless permanent magnet motor," *4th IET International Conference on Power Electronics, Machines and Drives*, pp. 707–711, 2008.

[31] M. Kang, J. Huang, H.-b. Jiang, *et al.*, "Principle and simulation of a 5-phase bearingless permanent magnet-type synchronous motor," in *2008 International Conference on Electrical Machines and Systems (ICEMS)*, IEEE, 2008, pp. 1148–1152.

[32] B. Li, J. Huang, M. Kang, *et al.*, "Analysis and simulation of a 7-phase pm bearingless motor," in *2011 International Conference on Electrical Machines and Systems (ICEMS)*, IEEE, 2011, pp. 1–5.

[33] J. Huang, M. Kang, J.-q. Yang, *et al.*, "Multiphase machine theory and its applications," in *2008 International Conference on Electrical Machines and Systems (ICEMS)*, IEEE, 2008, pp. 1–7.

[34] Z. Q. Zhu and D. Howe, "Instantaneous magnetic field distribution in brushless permanent magnet dc motors. II. armature-reaction field," *IEEE Transactions on Magnetics*, vol. 29, no. 1, pp. 136–142, 1993.

[35] Z. Liu, A. Chiba, Y. Irino, *et al.*, "Optimum pole number combination of a buried permanent magnet bearingless motor and test results at an output of 60 kw with a speed of 37000 r/min," *IEEE Open Journal of Industry Applications*, vol. 1, pp. 33–41, 2020.